Available online at www.sciencedirect.com
SCIENCE DIRECT
Thin Solid Films 506–507 (2006) 724 – 728
thin solid films
www.elsevier.com/locate/tsf

Modeling study of shrouding gas effects on a laminar argon plasma jet impinging upon a flat substrate in air surroundings

Kai Cheng [a], Xi Chen [a,*], Hai-Xing Wang [a], Wenxia Pan [b]

[a] *Department of Engineering Mechanics, Tsinghua University, Beijing 100084, PR China*
[b] *Institute of Mechanics, Chinese Academy of Sciences, Beijing 100080, PR China*

Available online 16 September 2005

Abstract

With the laminar plasma materials processing as the research background, modeling study is conducted concerning the effects of argon shroud on the characteristics of the *laminar* argon plasma jet impinging normally upon a flat substrate located in air surroundings. It is shown that adding shrouding gas is an effective method to reduce and control the entrainment of ambient air into the laminar plasma jet. The shrouding gas flow rate or velocity, the injection slot width and the stand-off distance of the substrate appreciably affect the air contents in the plasma near the substrate surface.

Keywords: Laminar plasma impinging jet; Shrouding gas; Species diffusion; Numerical method

1. Introduction

Thermal plasmas jets have been widely employed in materials processing, such as in the plasma spraying, surface cladding or re-melting hardening, etc. [1,2]. When the materials processing is performed in air surroundings, entrainment of ambient air into the plasma jet will inevitably lead to the oxidation of metallic particles injected into the plasma jet and/or of the metallic substrate (or workpiece) exposed to the plasma flow, while the material oxidation is often not desirable for many cases. Using a chamber filled with inert gas and enclosing the material processing system can avoid the unfavorable oxidation effects, but additional cost is often a limiting factor for its usage. Using gas shroud and/or solid shield is another possible choice to reduce the materials' oxidation. Refs. [3,4] presented some modeling results concerning the effects of the gas shroud and/or solid shield on the characteristics of *turbulent* plasma jets issuing into air surroundings. They showed that employing the gas shroud and/or solid shield can appreciably affect the temperature, velocity and air concentration fields in the turbulent plasma jets. Ref. [3] showed that in order to achieve a 'nearly oxygen-free plasma' region (air content ~10%) at 100 mm downstream from the nozzle exit, a shrouding gas (argon) flow rate 3.75 times as large as that of the torch working gas was required. Ref. [4] showed that employing a shrouding gas (same as the torch working gas) with a velocity of 100 m/s could reduce the air content from 82% to 46% at the turbulent jet center 105 mm downstream from the torch nozzle exit.

In recent years, stable long laminar plasma jets have been successfully generated with elaborately designed DC arc plasma torches [5–7]. In comparison with the turbulent plasma jets, the marked advantages of the long laminar plasma jet are that its emitted noise level is much lower; the entrainment of ambient gas into the plasma jet is significantly reduced since only molecular diffusion mechanism is involved for the laminar case; its high-temperature region length is much longer and can be easily adjusted by changing the arc current and/or working gas flow rate; and the axial gradients of plasma temperature and velocity are much smaller. These merits of the long laminar plasma jet make it very attractive from the viewpoint of materials processing

* Corresponding author. Fax: +86 10 62781824.
E-mail address: cx-dem@mail.tsinghua.edu.cn (X. Chen).

0040-6090/$ - see front matter © 2005 Elsevier B.V. All rights reserved.
doi:10.1016/j.tsf.2005.08.148

since it provides a new possibility to achieve low-noise working surroundings, better process repeatability and controllability, and reduced oxidation degree of metallic materials processed in air surroundings. Preliminary attempts [7,8] to use long laminar plasma jets in the preparation of thermal barrier coatings and in the re-melting hardening of cast iron and the stainless-steel surface cladding (with Ni+30%ZrO_2 powder addition) have shown encouraging results, including the fine microstructure, low surface roughness and small porosity of the prepared coatings, the good re-melting process controllability and surface morphologies, as well as the preferable metallurgically bonded clad layer.

Xu et al. [9] performed a three-dimensional modeling study concerning the characteristics of the long laminar argon plasma jet issuing into ambient air for the cases with or without lateral carrier-gas injection. Especially, they numerically studied the diffusion of the ambient air into the laminar argon plasma jet using the combined-diffusion-coefficient method [10,11]. Their modeling results showed that although the entrainment of ambient air into the laminar argon plasma jet was significantly less than that for the turbulent plasma jet case, considerably large air contents could still exist in the downstream region of the laminar argon plasma jet. Hence, for some practical applications, how to reduce and control the entrainment of ambient air into the laminar argon plasma jet is still a problem.

With the practical applications of the laminar plasma jet in materials processing (coating preparation, surface re-melting hardening, plasma surface cladding, etc.) as the research background, the effects of shrouding gas (argon) on the characteristics of the *laminar* argon plasma jet impinging normally upon a flat substrate located in air surroundings are numerically studied in this paper.

2. Modeling approach

Main assumptions and governing equations employed in this study are almost the same as those used in [9]. The assumptions include steady, laminar and axi-symmetrical flow with negligible swirling velocity component; local thermodynamic equilibrium (LTE) and optically thin plasma; the diffusion of ambient air into the plasma jet can be handled using the combined-diffusion-coefficient method [10,11]. The governing equations concerning the mass, momentum, energy, and gas species conservation in the cylindrical coordinate system are as follows:

$$\frac{\partial}{\partial x}(\rho u)+\frac{1}{r}\frac{\partial}{\partial r}(r\rho v)=0 \tag{1}$$

$$\frac{\partial(\rho uu)}{\partial x}+\frac{1}{r}\frac{\partial(r\rho uv)}{\partial r}=-\frac{\partial p}{\partial x}+2\frac{\partial}{\partial x}\left[\mu\frac{\partial u}{\partial x}\right]+\frac{1}{r}\frac{\partial}{\partial r}\left[r\mu\left(\frac{\partial u}{\partial r}+\frac{\partial v}{\partial x}\right)\right] \tag{2}$$

$$\frac{\partial(\rho uv)}{\partial x}+\frac{1}{r}\frac{\partial(r\rho vv)}{\partial r}=-\frac{\partial p}{\partial r}+\frac{2}{r}\frac{\partial}{\partial r}\left[r\mu\frac{\partial v}{\partial r}\right]+\frac{\partial}{\partial x}\left[\mu\left(\frac{\partial v}{\partial x}+\frac{\partial u}{\partial r}\right)\right]-2\mu\frac{v}{r^2} \tag{3}$$

$$\frac{\partial(\rho uh)}{\partial x}+\frac{1}{r}\frac{\partial(r\rho vh)}{\partial r}=\frac{\partial}{\partial x}\left[\frac{k}{c_p}\frac{\partial h}{\partial x}\right]+\frac{1}{r}\frac{\partial}{\partial r}\left[r\frac{k}{c_p}\frac{\partial h}{\partial r}\right]-U_r-\frac{\partial}{\partial x}[(h_A-h_B)J_x]-\frac{1}{r}\frac{\partial}{\partial r}[r(h_A-h_B)J_r]-\frac{\partial}{\partial x}\left[\frac{k}{c_p}(h_A-h_B)\frac{\partial f_A}{\partial x}\right]-\frac{1}{r}\frac{\partial}{\partial r}\left[r\frac{k}{c_p}(h_A-h_B)\frac{\partial f_A}{\partial r}\right] \tag{4}$$

$$\frac{\partial(\rho uf_A)}{\partial x}+\frac{1}{r}\frac{\partial(r\rho vf_A)}{\partial r}=\frac{\partial}{\partial x}\left[\Gamma_f\frac{\partial f_A}{\partial x}\right]+\frac{1}{r}\frac{\partial}{\partial r}\left[r\Gamma_f\frac{\partial f_A}{\partial x}\right]+S_f \tag{5}$$

Here u and v are the axial ($x-$) and radial ($r-$) velocity components; ρ, μ, k, c_p, h and U_r are temperature- and composition-dependent plasma density, viscosity, thermal conductivity, specific heat at constant pressure, specific enthalpy and radiation power per unit volume of plasma, respectively; p the pressure, whereas f_A is the mass fraction of argon species in the argon–air mixture. In Eq. (4), h_A and h_B are the specific enthalpies of gases A (argon) and B (air), respectively, whereas J_x and J_r are the axial ($x-$) and radial ($r-$) components of the argon diffusion mass flux vector [10,11] $\overline{J}_A=-(n^2/\rho)\overline{m}_A\overline{m}_B\overline{D}^x_{AB}\nabla X_A-\overline{D}^T_{AB}\nabla\ln T$. Here n is the total gas-particle number density, $\overline{m}_A$ and $\overline{m}_B$ are the averaged particle masses for all the *heavy* gas particles (excluding electrons) coming from argon and those from air, X_A is the mole fraction of argon in the argon–air mixture, whereas $\overline{D}^x_{AB}$ and $\overline{D}^T_{AB}$ are the combined ordinary diffusion coefficient associated with the argon mole-concentration gradient ∇X_A and the combined thermal diffusion coefficient associated with the temperature gradient ∇T, respectively [10,11]. The transport coefficient in Eq. (5) is expressed by $\Gamma_f=\left[\overline{m}_A\overline{m}_B/\left(\overline{M}\overline{M}_A\right)\right]\rho\overline{D}^x_{AB}$, in which $\overline{M}$ and $\overline{M}_A$ are the averaged gas-particle mass for *all* the gas particles (including electrons) of the gas mixture and that for *all* the gas particles coming from argon, respectively, whereas the source term S_f is [9]

$$S_f=\frac{\partial}{\partial x}\left(\Gamma_f\frac{f_A}{\overline{M}}\frac{\partial\overline{M}}{\partial x}\right)-\frac{\partial}{\partial x}\left(\Gamma_f\frac{f_A}{\overline{M}_A}\frac{\partial\overline{M}_A}{\partial x}\right)+\frac{1}{r}\frac{\partial}{\partial r}\left(r\Gamma_f\frac{f_A}{\overline{M}}\frac{\partial\overline{M}}{\partial r}\right)-\frac{1}{r}\frac{\partial}{\partial r}\left(r\Gamma_f\frac{f_A}{\overline{M}_A}\frac{\partial\overline{M}_A}{\partial r}\right)+\frac{\partial}{\partial x}\left(\overline{D}^T_{AB}\frac{\partial\ln T}{\partial x}\right)+\frac{1}{r}\frac{\partial}{\partial r}\left(r\overline{D}^T_{AB}\frac{\partial\ln T}{\partial r}\right) \tag{6}$$

The computational domain employed in this study is the region A–J–K–L–A shown in Fig. 1, i.e. the upper semi-plane of the axi-symmetrical impinging jet. The left-hand side of plane N–D–E is the plasma torch with A–B being the plasma flow inlet, B–C–D is a backward-step region, whereas N–D is the torch outlet. E–F represents the annular slot for the shrouding gas (argon) injection, and F–G–H–I is the wall of outer hood to constrict the shrouding gas. L–K is the substrate surface, whereas I–J and J–K are the left and top free boundaries, respectively.

In the computation, the radial size (AJ) of the computational domain is set 50 mm, whereas axial size AL is 18 mm or 45 mm. Other sizes adopted are as follows: inner radius of plasma flow inlet (AB) is 2 mm, torch exit inner radius (ND) 4 mm, wall thickness (BI) 33 mm, backward-step length (CD) 8 mm, height of the left free boundary (IJ) 15 mm, slot width for the shrouding gas injection (EF) can be 0.2, 0.5 or 1 mm. A non-uniform 92 $(x-)\times 187$ $(r-)$ mesh is employed in the computation with fine mesh spacing near the jet axis and shrouding gas injection slot.

The boundary conditions used in modeling include that at the jet inlet A–B, $v=0$, $f_A=1.0$, and the following profiles of axial velocity and temperature are used:

$$u = U_0\left[1-(r/R_{in})^{1.4}\right],$$
$$T = (T_0 - T_w)\left[1-(r/R_{in})^{2.3}\right] + T_w \quad (7)$$

in which U_0 and T_0 are the maximum axial velocity and temperature (correspondent specific enthalpy can be easily calculated) at jet axis, T_w is the inner wall temperature of plasma torch, and $T_w=700$ K; axi-symmetrical conditions $\partial\phi/\partial r=0$ ($\phi=u$, h, f_A) and $v=0$ are employed along the jet axis A–L; a fixed axial velocity (or argon flow rate) and $v=0$, $T=300$ K, $f_A=1.0$ are used at the outlet of shrouding gas slot (E–F); free boundary conditions are employed along I–J and J–K; $u=v=0$, fixed temperature and zero diffusion flux are used at the solid wall. The SIMPLE-like algorithm has been employed to solve the governing equations associated with corresponding boundary conditions.

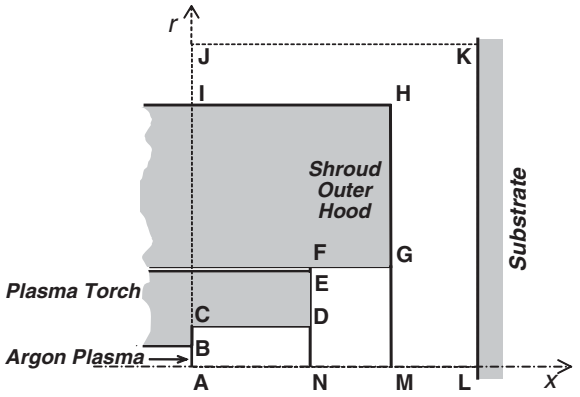

Fig. 1. Computational domain used in this study.

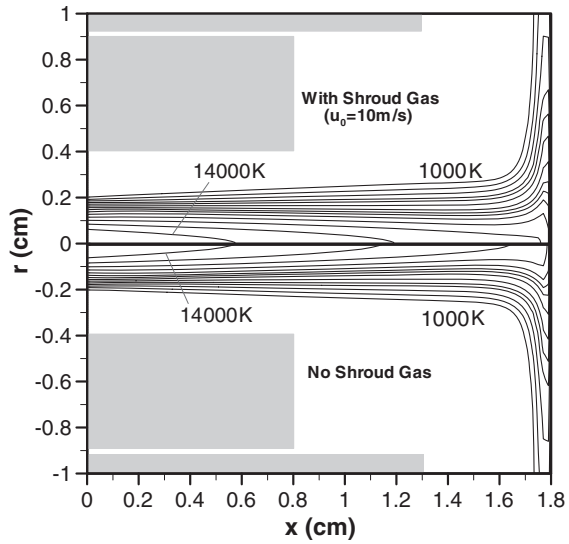

Fig. 2. Comparison of computed temperature fields in the impinging jet. Upper semi-plane: shrouding gas velocity of 10 m/s; lower semi-plane: without gas shroud. Outer isotherm — 1000 K, isotherm interval — 1000 K.

3. Results and discussion

Typical computed results are presented in Figs. 2–5 for the case with $U_0=800$ m/s (corresponding to argon mass flow rate $G_0=0.196$ g/s) and $T_0=15\,000$ K in Eq. (7), substrate stand-off distance (AL in Fig. 1) 18 mm, shrouding gas slot width (EF) 0.2 mm and radial location (NE) 9.2 mm, and outer hood extension length (FG) 5 mm.

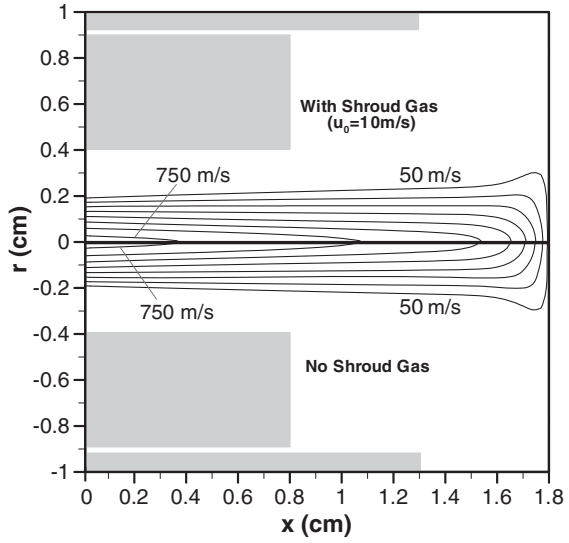

Fig. 3. Comparison of computed axial-velocity distributions in the impinging jet. Upper semi-plane: shrouding gas velocity of 10 m/s; lower semi-plane: without gas shroud. Outer contour — 50 m/s, contour interval — 100 m/s.

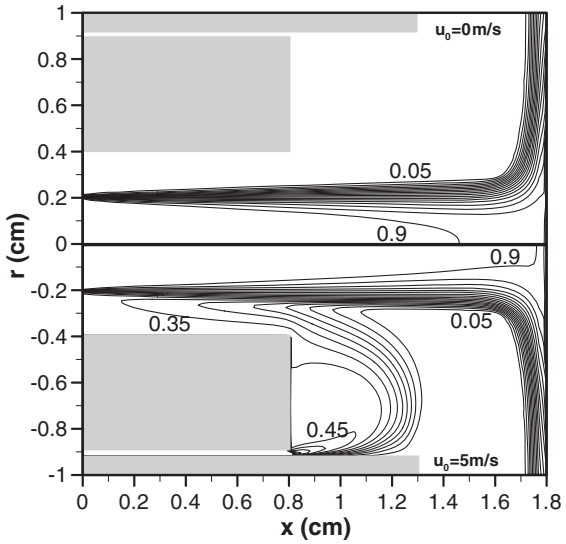

Fig. 4. Comparison of computed argon mass fraction distributions in the impinging jet. Upper semi-plane: without gas shroud; lower semi-plane: shrouding gas velocity of 5 m/s. Outer contour — f_A=0.05, contour interval — 0.05.

The values of U_0 and T_0 are taken based on measured data. Fig. 2 compares the computed temperature distributions in the impinging plasma jet for the cases with and without shrouding gas injection (u_0=10 m/s for upper semi-plane and u_0=0 m/s for lower semi-plane). Corresponding computed results of the axial velocity distributions are compared in Fig. 3. It can be seen from Figs. 2 and 3 that the shrouding gas injection only slightly affects the temperature and flow fields in the central region of plasma jet. Fig. 4 compares the computed distributions of argon mass fraction for the cases without and with shrouding gas injection (u_0=0 m/s for upper semi-plane and u_0=5 m/s for lower semi-plane). It is seen that the addition of shrouding gas (argon) appreciably affects the argon mass fraction (f_A) distribution in the impinging jet, and the value of oxygen mass fraction (calculated from $f_{ox}=0.23\times(1-f_A)$) at the substrate surface center (at point L in Fig. 1) decreases from 2.76% for u_0=0 m/s to 2.28% for u_0=5 m/s. Fig. 5 compares the computed distributions of argon mass fraction for the cases for two different shrouding gas velocities. It is seen that although increasing the shrouding gas velocity from 10 m/s to 20 m/s can still affect the argon mass fraction distribution in the outer region the plasma jet, the value of air mass fraction f_B at the substrate surface center is less influenced (f_{ox} only decreases from 2.18% for u_0=10 m/s to 2.16% for u_0=20 m/s). Corresponding to the different shrouding argon flow rates 0 g/s, 0.093 g/s (u_0=5 m/s), 0.185 g/s (u_0=10 m/s), 0.279 g/s (u_0=15 m/s) and 0.371 g/s (u_0=20 m/s), i.e. for the ratios of the shrouding argon mass flow rate to the mass flow rate of torch working gas (argon) being 0, 0.47, 0.94, 1.41 and 1.89, the computed values of oxygen mass fraction (f_{ox}) at the substrate center are 2.76%, 2.28%, 2.18%, 2.16% and 2.16%, respectively. The predicted results demonstrate that when the shrouding gas velocity increases from 0 to 5 or 10 m/s, the effect of the shrouding gas velocity on the oxygen mass fraction is appreciable. Further increase of the shrouding gas velocity less affects the values of oxygen mass fraction (f_{ox}) at the substrate surface center, although the f_{ox} values in the outer region at the substrate surface can still be slightly reduced.

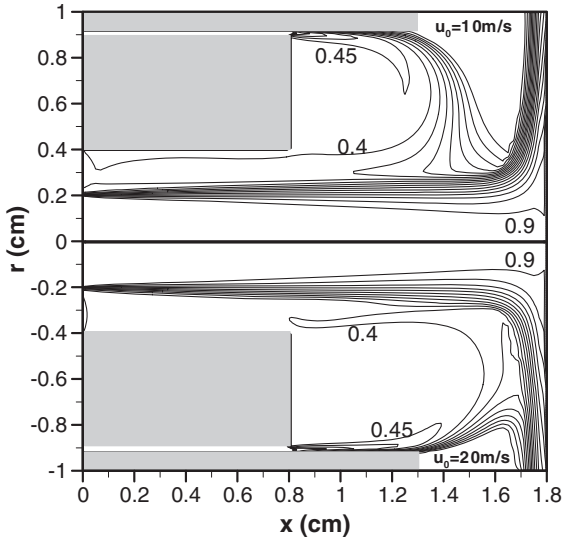

Fig. 5. Comparison of computed argon mass fraction distributions in the impinging jet. Upper semi-plane: shrouding gas velocity of 10 m/s; lower semi-plane: shrouding gas velocity of 20 m/s. Outer contour — f_A=0.05, contour interval — 0.05.

Computed results are presented in Table 1 concerning the effects of the shrouding argon mass flow rate on the value of oxygen mass fraction (f_{ox}) at the substrate surface center for three different shroud gas slot widths (i.e. 0.2, 0.5 and 1.0 mm). It is seen from Table 1 that for a given shrouding gas flow rate, the computed f_{ox} values are almost the same for the cases with EF=0.5 and 1.0 mm, while the computed f_{ox} values for the case with EF=0.2 mm are somewhat larger, although the shrouding gas velocity appreciably decreases with increasing slot width for a fixed flow rate. Increasing the shroud gas slot width from 0.2 mm to 0.5 mm is beneficial, but further increase of the slot width is not justified.

With coating preparation as the research background, computational studies are also conducted for the case with the substrate stand-off distance (AL) equaling 45 mm. The mass flow rate of the working gas in the plasma torch is

Table 1
Variations of the oxygen mass fraction at the substrate surface center with the mass flow rate of the shrouding gas for three different slot widths (EF=0.2, 0.5 and 1.0 mm, AL=18 mm)

Slot width EF (mm)	Shroud gas mass flow rate (g/s)				
	0	0.093	0.186	0.279	0.371
0.2	2.76%	2.28%	2.18%	2.16%	2.16%
0.5	2.76%	2.16%	2.00%	1.98%	1.98%
1.0	2.76%	2.16%	1.95%	1.96%	1.96%

U_0=800 m/s and T_0=15000 K.

Table 2
Variations of the oxygen mass fraction at the substrate surface center with the mass flow rate of the shrouding gas for the case with substrate stand-off distance AL=45 mm

Shrouding gas mass flow rate (g/s)	0	0.093	0.186	0.371	0.558
Oxygen mass fraction (%)	4.02	3.50	2.93	2.36	2.31

U_0=1200 m/s and T_0=15000 K.

taken to be 0.294 g/s (U_0=1200 m/s), the shroud gas slot width EF is 0.2 mm, whereas the mass flow rate of the shroud gas is 0 g/s, 0.093 g/s (u_0=5 m/s), 0.186 g/s (u_0=10 m/s), 0.371 g/s (u_0=20 m/s) or 0.558 g/s (u_0=30 m/s). Typical predicted results are presented in Table 2 concerning the values of the oxygen mass fraction (f_{ox}) at the substrate surface center for those different shrouding gas flow rates. Appreciable effects of the shroud gas injection on the computed argon mass fraction distributions are clearly seen. From Table 2, similar conclusion can be drawn as that for the case with substrate stand-off distance AL=18 mm given in Table 1, i.e. appropriate increase of the shroud gas flow rate is beneficial, but too large flow rate (e.g. >0.558 g/s) of the shroud gas is not necessary.

4. Summary

Modeling results are presented concerning the effects of coaxial gas shroud on the diffusion of ambient air (or oxygen) into the laminar argon plasma impinging jet. It is shown that the gas shroud only slightly affects the flow and temperature fields in the central region of plasma jet; increasing the shroud gas velocity or slot width within a suitable range can reduce the air contents near the substrate surface center; and the substrate stand-off distance significantly affects the air entrainment.

Acknowledgement

This study was supported by the National Natural Science Foundation of China (Nos. 50336010, 10405015 and 50276065). The authors would like to thank Dr. A. B. Murphy, whose argon–air plasma properties have been used in this study.

References

[1] E. Pfender, Plasma Chem. Plasma Process. 19 (1999) 1.
[2] P. Fauchais, J. Phys. D: Appl. Phys. 37 (2004) R86.
[3] K.D. Kang, S.H. Hong, J. Appl. Phys. 85 (1999) 6373.
[4] D.T. Gawne, T. Zhang, B. Liu, Surf. Coat. Technol. 153 (2002) 148.
[5] K. Osaki, O. Fukumasa, A. Kobayashi, Vacuum 59 (2000) 47.
[6] W.-X. Pan, W.-Hua Zhang, W.-Hong Zhang, C.-K. Wu, Plasma Chem. Plasma Process. 21 (2001) 23.
[7] W.-X. Pan, W.-H. Zhang, W. Ma, C.-K. Wu, Plasma Chem. Plasma Process. 22 (2002) 271.
[8] W.-X. Pan, W. Ma, C.-K. Wu, in: Y.-C. Zhou, et al., (Eds.), Mechanics and Material Engineering for Science and Experiments, Science Press, Beijing, 2003, p. 427.
[9] D.-Y. Xu, Xi Chen, K. Cheng, J. Phys. D: Appl. Phys. 36 (2003) 1583.
[10] A.B. Murphy, Phys. Rev., E 48 (1993) 3594.
[11] A.B. Murphy, J. Phys. D: Appl. Phys. 29 (1996) 1922.